Acta Crystallographica Section F
Structural Biology and Crystallization Communications
ISSN 1744-3091

Conformational change of the AcrR regulator reveals a possible mechanism of induction

Ruoyu Gu,[a]‡ Ming Li,[a]‡ Chih-Chia Su,[b] Feng Long,[c] Mathew D. Routh,[c] Feng Yang,[a] Gerry McDermott[d] and Edward W. Yu[a,b,c]*

[a]Department of Physics and Astronomy, Iowa State University, Ames, IA 50011, USA, [b]Department of Biochemistry, Biophysics and Molecular Biology, Iowa State University, Ames, IA 50011, USA, [c]Molecular, Cellular and Developmental Biology Interdepartmental Graduate Program, Iowa State University, Ames, IA 50011, USA, and [d]Department of Anatomy, School of Medicine, University of California, San Francisco, CA 94143, USA

‡ RG and ML contributed equally to this work.

Correspondence e-mail: ewyu@iastate.edu

Received 16 November 2007
Accepted 27 May 2008

PDB Reference: AcrR, 3bcg, r3bcgsf.

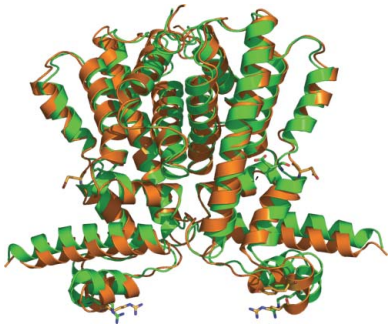

The *Escherichia coli* AcrR multidrug-binding protein represses transcription of *acrAB* and is induced by many structurally unrelated cytotoxic compounds. The crystal structure of AcrR in space group $P222_1$ has been reported previously. This $P222_1$ structure has provided direct information about the multidrug-binding site and important residues for drug recognition. Here, a crystal structure of this regulator in space group $P3_1$ is presented. Comparison of the two AcrR structures reveals possible mechanisms of ligand binding and AcrR regulation.

1. Introduction

The disturbing increase in multidrug resistance (MDR) observed in bacteria is a growing problem associated with the use of antibiotics for treating bacterial infections. Bacterial multidrug resistance is to a large extent attributed to the expression of multidrug efflux transporters that are capable of extruding a wide variety of toxic compounds from bacterial cells (Levy, 1992, 2001; Saier *et al.*, 1998; McKeegan *et al.*, 2003). *Escherichia coli* AcrB is one of the prototypical members of the resistance–nodulation–division (RND) family of transporters (Tseng *et al.*, 1999; Ma *et al.*, 1995). This inner membrane protein recognizes a variety of structurally dissimilar agents, including most currently used antibiotics, chemotherapeutic agents, detergents and dyes (Nikaido, 1996). In association with a periplasmic membrane-fusion protein, AcrA (Zgurskaya & Nikaido, 2000), and an outer membrane channel, TolC (Koronakis *et al.*, 2000), the AcrB multidrug efflux pump is capable of exporting these structurally dissimilar compounds directly to the external medium.

The transcription of *acrAB* is regulated by a global transcriptional activator, MarA, and a local transcriptional repressor, AcrR (Ma *et al.*, 1996). AcrR is a 215-amino-acid protein that belongs to the TetR family of transcriptional repressors (Ramos *et al.*, 2005). Recently, the ligand-free structure of AcrR has been determined in our laboratory (Li *et al.*, 2007). The crystal structure revealed that AcrR is a dimeric two-domain molecule with an entirely helical architecture, similar to other members of the TetR family. Each subunit of AcrR is composed of nine helices ($\alpha1$–$\alpha9$ and $\alpha1'$–$\alpha9'$, respectively). The smaller N-terminal domain comprises helices $\alpha1$–$\alpha3$, with $\alpha2$ and $\alpha3$ forming the helix–turn–helix (HTH) DNA-binding motif. The larger C-terminal domain consists of helices $\alpha4$–$\alpha9$. The C-terminal domain forms a large internal cavity that was suggested to serve as the multidrug-binding pocket. Inside the drug-binding pocket, a completely buried negatively charged residue, Glu67, was found to be critical for drug recognition (Li *et al.*, 2007).

In *E. coli*, AcrR acts as a moderator to maintain sufficient expression levels of AcrB for bacterial survival in varying environments. The induction of AcrR is triggered by many structurally unrelated compounds, which are also substrates of the AcrB efflux pump. How AcrR binds inducing ligands and regulates the expression of AcrB is still not clear. The hypothesis is that binding of drugs to the C-terminal ligand-binding domain of AcrR triggers a conformational

Table 1
Data-collection, phasing and structural refinement statistics.

	Native	SeMet, peak
Data collection		
Wavelength (Å)	0.9795	0.9795
Space group	$P3_1$	$P3_1$
Unit-cell parameters (Å)	$a = b = 46.7$, $c = 166.2$	$a = b = 46.6$, $c = 166.7$
Resolution (Å)	2.5 (2.57–2.48)	2.7 (2.84–2.74)
Completeness (%)	97.7 (84.5)	97.1 (91.1)
Total No. of reflections	466209	398102
No. of unique reflections	14362	11236
R_{merge} (%)	5.1 (24.4)	5.7 (11.8)
$\langle I/\sigma(I)\rangle$	23.2 (4.0)	45.4 (8.3)
Phasing		
Se-atom sites		14
Resolution range of data used (Å)		50–2.80
Overall figure of merit		0.39
Refinement		
R_{work} (%)	21.4	
R_{free} (%)	26.8	
Wilson B (Å^2)	62.6	
$\langle B\rangle$ (Å^2)	69.9	
R.m.s. deviations†		
Bond angles (°)	1.1	
Bond lengths (Å)	0.007	
Ramachandran analysis‡		
Most favored (%)	83.4	
Allowed (%)	14.7	
Generously allowed (%)	1.8	
Disallowed (%)	0.0	

† Engh & Huber (1991). ‡ Calculated using *PROCHECK* (Laskowski *et al.*, 1993).

change in the N-terminal DNA-binding region, which results in the release of AcrR from its operator DNA. Here, we report a new crystal structure of AcrR with space group $P3_1$, which is distinct from our previously reported $P222_1$ space-group structure. A comparison of these two structures reveals considerable conformational changes in both the N-terminal and C-terminal regions, suggesting that these two structures represent different conformational states of AcrR. These crystal structures provide novel insight into the mechanisms of ligand binding and AcrR regulation.

2. Materials and methods

2.1. Cloning, expression, purification, crystallization and data collection

Recombinant AcrR containing a 6×His tag at the C-terminus was expressed in *E. coli* using the pET15b vector. The cloning, expression and purification procedures have been described previously (Li *et al.*, 2006, 2007). For crystallization of native AcrR, a 4 µl drop consisting of 2 µl protein solution (20 m*M* Tris pH 7.5, 60 m*M* imidazole and 200 m*M* NaCl) and 2 µl well solution (34% PEG 3350, 3% MPD, 0.2 *M* $MgCl_2$ and 0.1 *M* Tris buffer pH 8.5) was equilibrated against 500 µl well solution. Under these conditions, a new bipyramidal crystal shape was obtained. The crystals were subsequently found to belong to space group $P3_1$. The SeMet-AcrR protein was crystallized under conditions identical to those used for native AcrR. The crystallization conditions provided sufficient cryoprotection and crystals were frozen directly in liquid nitrogen at 100 K. Diffraction data sets for both native and SeMet-AcrR were obtained at the Advanced Photo Source (APS, beamline 24IDC) at cryogenic temperature (100 K).

2.2. Structural determination and refinement

Diffraction data sets were processed with *DENZO* and scaled with *SCALEPACK* (Otwinowski & Minor, 1997). In order to avoid any model bias from using the $P222_1$ structure of AcrR in molecular replacement, we determined the new $P3_1$ structure of AcrR using single-wavelength anomalous dispersion (SAD). The native and SeMet crystals both belonged to space group $P3_1$; unit-cell parameters are summarized in Table 1. Following refinement of all 14 selenium sites of the AcrR dimer, initial phases were obtained by SAD using the program *BnP* (Weeks *et al.*, 2005). The electron-density map was then subjected to density modification (DM) and the initial model was obtained by the auto-interpretation routine function in the program *RESOLVE* (Terwilliger, 2001). After obtaining the initial model, the program *O* (Jones *et al.*, 1991) was used to perform manual model building. The model was then refined against the native data at 2.5 Å resolution using the programs *CNS* (Brünger *et al.*, 1998) and *REFMAC*5 (Collaborative Computational Project, Number 4, 1994; Murshudov *et al.*, 1997). Solvent atoms were initially built using the program *ARP*/*wARP* (Collaborative Computational Project, Number 4, 1994; Lamzin & Wilson, 1993) and subsequently added or removed by manual inspection. The final R_{work} and R_{free} (calculated using 5% of reflections omitted from the refinement) were 21.4% and 26.8%, respectively.

2.3. Protein Data Bank accession code

Coordinates and structural factors for the structure of AcrR have been deposited in the RCSB Protein Data Bank with accession code 3bcg.

3. Results and discussion

3.1. N-terminal DNA-binding domain

The overall structure of AcrR in space group $P3_1$ is very similar to the previously reported $P222_1$ space-group structure (PDB code 2qop) at 2.5 Å resolution determined recently in our laboratory (Li *et al.*, 2007). Superimposition of these two dimeric structures gives an overall r.m.s.d. of 1.4 Å calculated over the C^α atoms. However, a detailed comparison reveals a significant conformational change in the N-terminal DNA-binding domain. Fig. 1 illustrates a super-

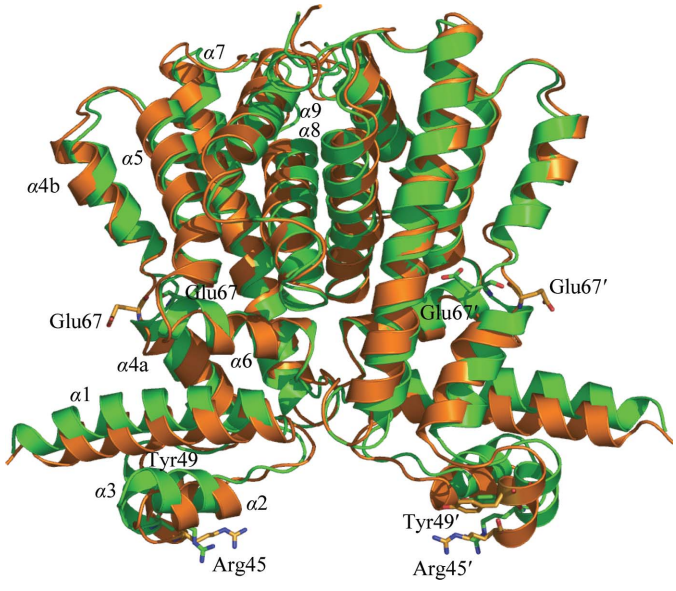

Figure 1
Structural comparison of the $P3_1$ and $P222_1$ structures of AcrR. Superimposition of the dimeric AcrR structures was performed using the program *ESCET* (orange, $P3_1$ structure; green, $P222_1$ structure).

position of these two AcrR structures using the program *ESCET* (Schneider, 2002). A plot of the distance between corresponding C^{α} atoms in the two dimeric AcrR structures with respect to residue number is shown in Fig. 2(*a*). The plot indeed suggests that the main difference in conformation between these two structures originates from helix α1 through the N-terminal half of helix α4. This change results in an overall r.m.s.d. of 2.8 Å for the C^{α} atoms in the N-terminal domains (residues 7–65), in contrast to the <0.7 Å r.m.s.d. of the C-terminal domains (residues 73–210). Fig. 2(*b*) illustrates an error-scaled distance difference matrix (*ESCET* plot; Schneider, 2002) calculated between the $P3_1$ and $P222_1$ structures.

Judging from the two crystal structures of AcrR, the conformational changes between the $P3_1$ and $P222_1$ structures seem to be predominantly rigid-body translation and rotation of the N-terminal domain. These movements lead to a downward shift of the entire N-terminal DNA-binding domain of the $P3_1$ structure (with respect to the orientation shown in Fig. 1) by 2.6 Å and a rotation of 10° towards the subunit interface of the dimer when compared with that of the $P222_1$ structure (Fig. 1). As a consequence of these movements, the two N-terminal domains of the AcrR dimer in the $P3_1$ structure

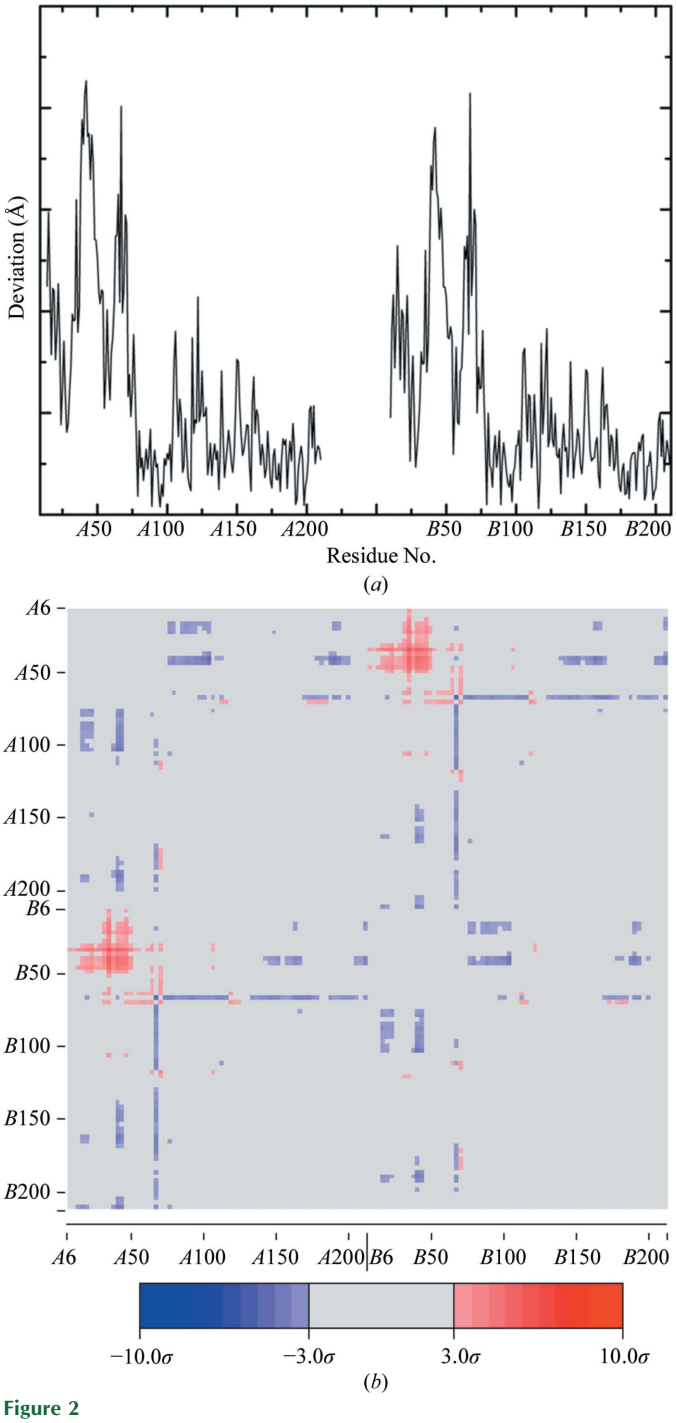

Figure 2
Structural rearrangement of the N-terminal domain of AcrR. (*a*) Plot of the distance between corresponding C^{α} atoms in AcrR after superposition of the dimeric $P3_1$ and $P222_1$ structures. (*b*) Error-scaled distance difference matrix (*ESCET* plot) calculated between the dimeric $P3_1$ and $P222_1$ AcrR structures.

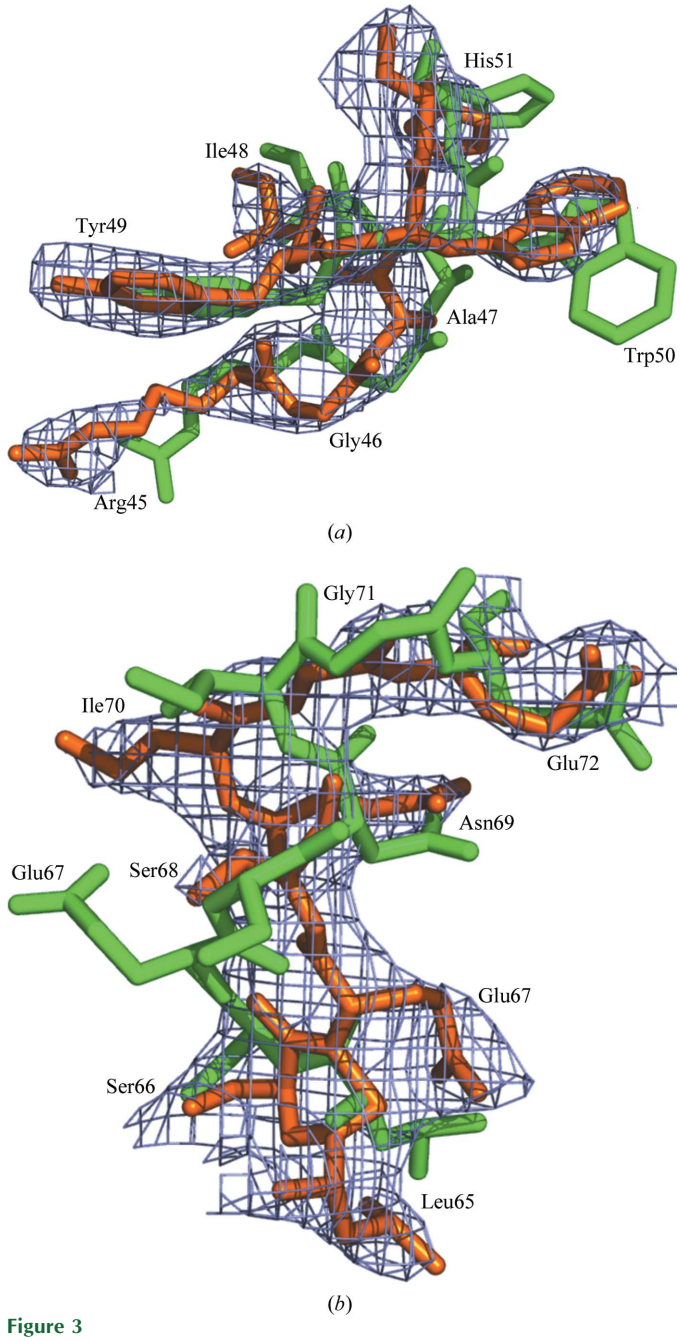

Figure 3
Electron-density maps of the $P3_1$ structure. (*a*) The $2F_{obs} - F_{calc}$ electron-density map (blue), contoured at 1.0σ, of the recognition helix α3 (orange, $P3_1$ structure; green, $P222_1$ structure). (*b*) The $2F_{obs} - F_{calc}$ electron-density map (blue), contoured at 1.0σ, of the flexible loop between helices α4a and α4b (orange, $P3_1$ structure; green, $P222_1$ structure).

come closer to each other by approximately 2 Å. The center-to-center distance between recognition helices $\alpha3$ and $\alpha3'$ (as measured by the distance between the C^{α} atoms of Tyr49 and Tyr49′) decreases from 42 Å in the $P222_1$ structure to 39 Å in the $P3_1$ structure. To bind two consecutive major grooves of B-DNA, the center-to-center distance has to be ∼34 Å. This distance is thought to increase upon drug binding, which in turn inhibits the binding of the regulator to its operator DNA. Thus, this center-to-center distance can reflect different conformational states of the regulator. For CmeR, the corresponding center-to-center distance was measured to be 54 Å. The relatively large center-to-center distance observed in CmeR suggested that CmeR was in a ligand-bound state (Gu *et al.*, 2007). In the case of QacR, the center-to-center distance is 39 Å for apo-QacR (Schumacher *et al.*, 2001). Upon DNA and drug binding to QacR, the corresponding center-to-center distances become 37 and 48 Å, respectively (Schumacher *et al.*, 2002). Because of these center-to-center distances, it is likely that the structure of the DNA-bound form of AcrR is more similar to the $P3_1$ structure, while its drug-bound form is more closely related to the $P222_1$ conformation.

In addition to these differences, Arg45, an N-terminal amino acid which has been identified to be indispensable for DNA binding and important for AcrR regulation (Webber & Piddock, 2001), undergoes a significant conformational change. The $C^{\alpha}-C^{\alpha}$ distance between Arg45 and Arg45′ decreases from 40 Å in the $P222_1$ structure to 35 Å in the $P3_1$ structure. A comparison of the conformation of helix $\alpha3$ in the two AcrR structures is shown in Fig. 3(*a*).

We analyzed the normal modes of vibration of the $P3_1$ structure of AcrR using the program *ElNémo* (Suhre & Sanejouand, 2004*a*,*b*). The results suggest that the lowest frequency nontrivial vibrational mode indeed corresponds to the swinging motion of the entire N-terminal DNA-binding domain. This swinging motion highlights the transition between the $P3_1$ and $P222_1$ structures. Accompanied by this N-terminal swinging motion, the COOH-terminus of helix $\alpha4a$ and the NH_2-terminus of helix $\alpha6$ perform helix-to-coil transitions in this vibrational mode. These shifts in conformation of helices $\alpha4$ and $\alpha6$ are also consistent with the observed difference between the two AcrR structures, as discussed below.

3.2. C-terminal regulatory domain

One unique feature found in the crystal structure of AcrR is the presence of a short loop in the middle of helix $\alpha4$. To better facilitate comparison with the structures of other TetR members, residues 55–65 and 69–80 in the $P222_1$ structure were assigned as helices $\alpha4a$ and $\alpha4b$, respectively (Li *et al.*, 2007). The short loop between $\alpha4a$ and $\alpha4b$ acts as a transition region connecting the N-terminal and C-terminal domains. In the $P222_1$ structure, this flexible loop consists of residues 66–68. In the $P3_1$ structure, however, this loop contains four more residues (66–72). Unlike the conformational change in the N-terminal domain, which is mainly an overall shift in position of the entire domain, the changes in the C-terminal domain of these two conformations are predominately associated with local movements of the flexible loop between $\alpha4a$ and $\alpha4b$ and helices $\alpha4$ and $\alpha6$.

It has been found that Glu67, a completely buried residue in the drug-binding pocket of the $P222_1$ structure, is critical for drug recognition (Li *et al.*, 2007). In the $P3_1$ structure, Glu67 is expelled from the hydrophobic core into the solvent (Figs. 1 and 3*b*). The shift in the C^{α} atom of this residue reaches 4.2 Å when compared with that of the $P222_1$ structure. In addition, the side chain of Glu67 flips away from the hydrophobic core of the drug-binding pocket. This results in a positional shift of the two carboxylate O atoms (OE1 and OE2) in the side chain of Glu67 by more than 10 Å when compared with those of the $P222_1$ structure. The nearby flexible-loop residues between $\alpha4a$ and $\alpha4b$ also shift considerably in response to this large movement (Fig. 3*b*). Coupled with the movement of Glu67, helix $\alpha4a$ shifts toward the N-terminal DNA-binding domain by 2.3 Å in the $P3_1$ structure when compared with the $P222_1$ structure (Fig. 1).

Comparison of the $P222_1$ and $P3_1$ structures also reveals conformational changes in helix $\alpha6$. Arg105 and Arg106 in the $P3_1$ structure shift in position, leading to an unwinding of the helical residues Glu104–Arg106 at the N-terminus of $\alpha6$. Thus, helix $\alpha6$ is shortened by one turn in the $P3_1$ structure. This change may be attributed to the movement of the flexible loop between $\alpha4a$ and $\alpha4b$. In the $P222_1$ structure, Arg106 is hydrogen bonded to Glu67 (Fig. 4). This hydrogen bond is missing in the $P3_1$ structure owing to the expulsion of Glu67 from the hydrophobic core. As a consequence, this motion induces a helix-to-coil transition of helix $\alpha6$. In addition to the above change, it was found that Arg105 is hydrogen bonded to residues Gln14 and Asp18 in the $P222_1$ structure (Fig. 4). These hydrogen bonds are also missing in the $P3_1$ structure.

Based on the $P3_1$ and $P222_1$ structures of AcrR, we suspect that the changes in the conformation of the N-terminal DNA-binding and C-terminal drug-binding domains of AcrR are cooperative owing to the formation of hydrogen bonds at the interface between these two domains (Fig. 4). In the DNA-bound form of AcrR, the structure of the regulator may be closer to the $P3_1$ structure. Thus, the side chain of Glu67 may point outside the drug-binding pocket and be exposed to the solvent. Drug binding to the C-terminal domain may induce conformational changes that result in a conformation more closely related to the $P222_1$ structure, in which the side chain of Glu67 flips into the interior of the hydrophobic core. This change may also be accompanied by the formation of new hydrogen bonds between Glu67 and Arg106, Arg105 and Gln14, and Arg105 and Asp18. The

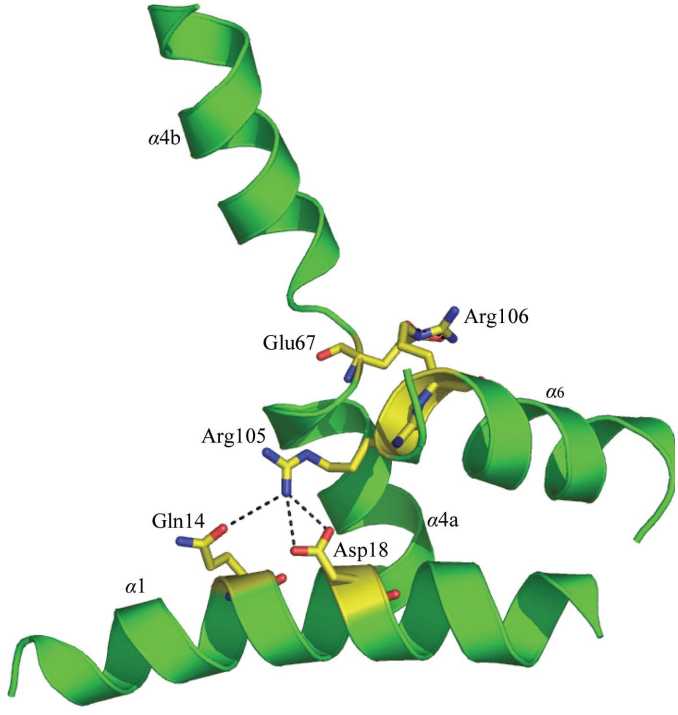

Figure 4
Hydrogen bonds at the interface between the C-terminal and N-terminal domains of one subunit of the $P222_1$ structure of AcrR. The hydrogen bonds, shown as dotted lines, are between Glu67 and Arg106, between Gln14 and Arg105 and between Asp18 and Arg105. These hydrogen bonds are absent in the $P3_1$ structure. The orientation of this figure is the same as that of Fig. 1.

crystal structures of both DNA-bound and drug-bound AcrR would be necessary to confirm the change in conformation upon DNA and drug binding.

This work is based upon research conducted at the Northeastern Collaborative Access Team beamlines of the Advanced Photon Source, supported by award RR-15301 from the National Center for Research Resources at the National Institutes of Health. Use of the Advanced Photon Source is supported by the US Department of Energy, Office of Basic Energy Sciences under Contract No. DE-AC02-06CH11357. This work was supported by a National Institutes of Health Grant GM074027 (to EWY). MDR is a recipient of a Roy J. Carver Trust predoctoral training fellowship.

References

Brünger, A. T., Adams, P. D., Clore, G. M., DeLano, W. L., Gros, P., Grosse-Kunstleve, R. W., Jiang, J.-S., Kuszewski, J., Nilges, M., Pannu, N. S., Read, R. J., Rice, L. M., Simonson, T. & Warren, G. L. (1998). *Acta Cryst.* D**54**, 905–921.

Collaborative Computational Project, Number 4 (1994). *Acta Cryst.* D**50**, 760–763.

Engh, R. A. & Huber, R. (1991). *Acta Cryst.* A**47**, 392–400.

Gu, R., Su, C.-C., Shi, F., Li, M., McDermott, G., Zhang, Q. & Yu, E. W. (2007). *J. Mol. Biol.* **372,** 583–593.

Jones, T. A., Zou, J.-Y., Cowan, S. W. & Kjeldgaard, M. (1991). *Acta Cryst.* A**47**, 110–119.

Koronakis, V., Sharff, A., Koronakis, E., Luisi, B. & Hughes, C. (2000). *Nature (London)*, **405**, 914–919.

Lamzin, V. S. & Wilson, K. S. (1993). *Acta Cryst.* D**49**, 129–147.

Laskowski, R. A., MacArthur, M. W., Moss, D. S. & Thornton, J. M. (1993). *J. Appl. Cryst.* **26**, 283–291.

Levy, S. B. (2001). *Clin. Infect. Dis.* **33**, *Suppl.* 3, S124–S129.

Levy, S. B. (1992). *Antimicrob. Agents Chemother.* **36**, 695–703.

Li, M., Gu, R., Su, C.-C., Routh, M. D., Harris, K. C., Jewell, E. S., McDermott, G. & Yu, E. W. (2007). *J. Mol. Biol.* **374**, 591–603.

Li, M., Qiu, X., Su, C.-C., Long, F., Gu, R., McDermott, G. & Yu, E. W. (2006). *Acta Cryst.* F**62**, 1150–1152.

Ma, D., Alberti, M., Lynch, C., Nikaido, H. & Hearst, J. E. (1996). *Mol. Microbiol.* **19**, 101–112.

Ma, D., Cook, D. N., Alberti, M., Pon, N. G., Nikaido, H. & Hearst, J. E. (1995). *Mol. Microbiol.* **16**, 45–55.

McKeegan, K. S., Borges-Walmsley, M. I. & Walmsley, A. R. (2003). *Trends Microbiol.* **11**, 21–29.

Murshudov, G. N., Vagin, A. A. & Dodson, E. J. (1997). *Acta Cryst.* D**53**, 240–255.

Nikaido, H. (1996). *J. Bacteriol.* **178**, 5853–5859.

Otwinowski, Z. & Minor, W. (1997). *Methods Enzymol.* **276**, 307–326.

Ramos, J. L., Martínez-Bueno, M., Molina-Henares, A. J., Terán, W., Watanabe, K., Zhang, X., Gallegos, M. T., Brennan, R. & Tobes, R. (2005). *Microbiol. Mol. Biol. Rev.* **69**, 326–356.

Saier, M. H. Jr, Paulsen, I. T., Sliwinski, M. K., Pao, S. S., Skurray, R. A. & Nikaido, H. (1998). *FASEB J.* **12**, 265–274.

Schneider, T. R. (2002). *Acta Cryst.* D**58**, 195–208.

Schumacher, M. A., Miller, M. C., Grkovic, S., Brown, M. H., Skurray, R. A. & Brennan, R. G. (2001). *Science*, **294**, 2158–2163.

Schumacher, M. A., Miller, M. C., Grkovic, S., Brown, M. H., Skurray, R. A. & Brennan, R. G. (2002). *EMBO J.* **21**, 1210–1218.

Suhre, K. & Sanejouand, Y.-H. (2004*a*). *Nucleic Acids Res.* **32**, W610–W614.

Suhre, K. & Sanejouand, Y.-H. (2004b). *Acta Cryst.* D**60**, 796–799.

Terwilliger, T. C. (2001). *Acta Cryst.* D**57**, 1755–1762.

Tseng, T. T., Gratwick, K. S., Kollman, J., Park, D., Nies, D. H., Goffeau, A. & Saier, M. H. Jr (1999). *J. Mol. Microbiol. Biotechnol.* **1**, 107–125.

Webber, M. A. & Piddock, L. J. V. (2001). *Antimicrob. Agents Chemother.* **45**, 1550–1552.

Weeks, C. M., Shah, N., Green, M. L., Miller, R. & Furey, W. (2005). *Acta Cryst.* A**61**, C152.

Zgurskaya, H. I. & Nikaido, H. (2000). *J. Bacteriol.* **182**, 4264–4267.